photonics

MDPI

Article

5.3 W/265 μJ Mid-IR All-Fiber Er^{3+}:ZBLAN Gain-Switched Laser Based on Dielectric Fiber Mirror and Fiber-Tip Protection

Tingting Chen [1], Jue Su [1], Wenbo Zhong [2], Yu Ding [3], Lu Huang [1], Yikun Bu [1], Jianfeng Li [2] and Zhengqian Luo [1,*]

[1] Fujian Key Laboratory of Ultrafast Laser Technology and Applications, School of Electronic Science and Engineering, Xiamen University, Xiamen 361005, China
[2] State Key Laboratory of Electronic Thin Films and Integrated Devices, School of Optoelectronic Science and Engineering, University of Electronic Science and Technology of China (UESTC), Chengdu 610054, China
[3] Science and Technology on Electro-Optical Information Security Control Laboratory, Tianjin 300308, China
* Correspondence: zqluo@xmu.edu.cn

Abstract: We report a 2.8 μm all-fiber high-power and high-energy gain-switched Er^{3+}:ZBLAN laser based on dielectric fiber mirror and fiber-tip protection. The fiber pigtail mirror, specifically designed for dichroic operation (i.e., anti-reflection at 976 nm pump wavelength and high-reflection around 2.8 μm laser wavelength), shows high damage density of >10 MW/cm^2. An anti-reflection protective film is coated on the input tip of Er^{3+}:ZBLAN fiber and an AlF_3 endcap is spliced to the output tip of Er^{3+}:ZBLAN fiber for mitigating the fiber-tip photodegradation and high-power catastrophic failure at 2.8 μm. The compact all-fiber cavity is formed by efficiently connecting the Er^{3+}:ZBLAN fiber with dielectric fiber mirror using the standard FC/PC fiber adaptor. When the 976 nm pump operates in pulsed regime, the all-fiber mid-infrared gain-switched laser can be attained with two states of single-pulse and pulse-burst output. The extracted maximum pulse energy is 4.8 μJ in the single-pulse state, and the shortest pulse width is 426 ns. The pulse-burst mode can generate a maximum average power of 5.291 W and burst energy of 264.55 μJ. This work may offer a promising way to realize the low-cost, all-fiber, high-power and high-energy gain-switched laser at MIR wavelengths.

Keywords: mid-infrared gain-switched fiber laser; fiber mirror; high power

Citation: Chen, T.; Su, J.; Zhong W.; Ding, Y.; Huang, L.; Bu, Y.; Li, J.; Luo, Z. 5.3 W/265 μJ Mid-IR All-Fiber Er^{3+}:ZBLAN Gain-Switched Laser Based on Dielectric Fiber Mirror and Fiber-Tip Protection. *Photonics* **2024**, *11*, 700. https://doi.org/10.3390/photonics11080700

Received: 20 June 2024
Revised: 12 July 2024
Accepted: 25 July 2024
Published: 28 July 2024

1. Introduction

Mid-infrared (MIR) pulsed lasers emitting at ~3 μm waveband have attracted increasing attention in a variety of applications, such as material processing [1–4], Lidar [5–7], biomedical science [8–10], and infrared countermeasures [11,12], greatly promoting momentum in power scaling and pulse operation. Specifically, a pulsed laser source with high pulse energy and high repetition rate plays a key role in laser jamming on infrared seekers of air-defense missiles [12]. The microsecond pulsed laser, which uses a water vapor channel created by the leading part of the laser pulse, is the best choice for non-contact arthroscopic meniscectomy in a liquid environment [10]. The MIR pulse-burst laser has also been shown not only to optimize ablation-cooled efficiency and quality in biomaterial processing [4], but also to improve the echo-signal-to-noise ratio in differential absorption Lidar [6]. To date, Q-switching [13–21] and gain-switching [22–32] have been regarded as the two most efficient methods to attain nanosecond/millisecond-scale short pulses with high energy. Q-switching based on the acousto-optic modulator [13], electric-optic modulator [14–17], or saturable absorbers [18–21] has been used in the typical MIR pulsed lasers, but usually suffers from challenges in compactness, cost, and stability. In contrast, gain-switching provides an alternative method for pulse generation with advantages of simple structure and high performance, because it can quickly modulate the laser gain by only pump modulation. The realization of gain-switched operation in fiber lasers, especially in rare-earth-doped fiber lasers, is extremely convenient due to their high optical gain and robust architecture.

In the past two decades, MIR gain-switched operations in rare-earth-ion (Er^{3+} [22–27], Dy^{3+} [28–30], Ho^{3+} [31,32])-doped fluoride-glass fiber lasers have been demonstrated with remarkable results Appendix A. Since 2001, the first 2.8 μm gain-switched Er^{3+}-doped ZBLAN fiber laser pumped by Ti:sapphire laser was reported [22]. By introducing fast gain-switching to regulate the chaotic spikes, the 2.8 μm single-pulse gain-switched Er^{3+}:ZBLAN fiber laser was reported in 2011, enabling a maximum average (peak) power of 2 W (68 W), slope efficiency of 34%, and a pulse width of ∼300 ns [23]. Dy^{3+}- [28–30] and Ho^{3+} [31]-doped ∼3 μm gain-switched ZBLAN fiber lasers with extended tunable range and switchable temporal states have been demonstrated recently. However, due to the lack of MIR fiberized components, almost all of the previously reported MIR gain-switched fiber lasers use some free-space optical components; such a non-all-fiber structure may undermine the robustness and reliability of the fiber lasers. Up until now, only a few reports have realized ∼3 μm gain-switched all-fiber lasers [24,32]. In 2018, a record 2.83 μm all-fiber gain-switched Er^{3+}:ZBLAN fiber laser using mid-infrared fiber Bragg grating (FBG) fabrication technique was reported by Paradis, and the average power was 11.2 W with a pulse width of 170 ns and a repetition rate of 140 kHz [24]. Nevertheless, the method for producing MIR all-fiber cavity above requires both of the femtosecond-written FBGs on the fluoride fiber and the low-loss fusion splicing between fluoride fibers, and thus, it is highly difficult and challenging in terms of technology. Therefore, it is necessary to develop an alternative solution for compact all-fiber gain-switched laser with low cost and easy availability. In addition, one should notice that the photodegradation and catastrophic fiber-tip damage in the case of ∼3 μm high-power output would be intensified by strong vapor absorption [33], threatening the laser output performance and thermo-mechanical stability. The nitrogen purged enclosure [34] and vacuum enclosure [35] have been proposed to alleviate the problem, but these lead to a complicated system. Therefore, there is strong motivation to develop new a technique for fiber-tip protection for MIR all-fiber large-energy pulse generation.

Herein, we put forward and experimentally demonstrated a 2.8 μm all-fiber gain-switched Er^{3+}:ZBLAN laser using MIR dielectric fiber mirror and fiber-tip protection. To begin, we specially designed and prepared a home-made high-damage fiber pigtail mirror (FPM) as the input mirror of the MIR resonant cavity. Following that, an anti-reflection (AR) protective film coated on the input tip of Er^{3+}:ZBLAN fiber was used to isolate the vapor absorption for preventing fiber-tip photodegradation. Meanwhile, an AlF_3-based endcap is fusion-spliced to the output tip of Er^{3+}:ZBLAN fiber, further improving the output power and operational stability. Using the scheme above, we finally demonstrated a compact MIR all-fiber high-power and high-energy gain-switched Er^{3+}:ZBLAN laser with two kinds of output states. The first is the state of a single short pulse, and 4.8 μJ/426 ns was obtained with repetition rate of 5 kHz. The other is the state of pulse burst (20 kHz), emitting maximum average power (maximum energy) of 5.291 W (264.55 μJ) with a slope efficiency of ∼25.2%.

2. Experimental Setup

The experimental setup is shown in Figure 1. Using a 976 nm pump laser, a high-reflectivity FPM (M1), an Er^{3+}:ZBLAN double-clad (DC) fiber, a protective film, and an AlF_3-based fiber endcap, the MIR laser cavity is constructed. The pump laser from a 976 nm pigtail laser diode (LD) can provide the maximum power of 27 W, and it has adjustable repetition rate (20 Hz–20 kHz) and pulse width (16–47 μs). The ∼3.1 m fiber manufactured by Le Verre Fluoré has a Er^{3+} doping concentration of 70,000 ppm, a 15 μm core diameter, a 0.12 numerical aperture of fiber core, 240/260 μm inner cladding (double D-shaped), and 285 μm outer cladding diameter, respectively. The home-made fusion-spliced M1 with 976 nm LD pigtail is connected with the Er^{3+}:ZBLAN fiber by FC/PC fiber adaptor, realizing the low-loss all-fiber coupling. An AR-600 nm-Ta_2O_5 layer is coated on the input tip of the Er^{3+}:ZBLAN fiber as a protective film. An AlF_3-based endcap fabricated by FiberLabs Inc. has 200/240 μm core/cladding diameter, and is fusion-spliced to the output tip of the Er^{3+}:ZBLAN fiber with low loss by using a fusion splicer LFS4100

(Vytran). The compact fiber linear cavity for 2.8 μm oscillation is formed by the M1 and ~3.5% Fresnel reflection of the output AlF_3-based endcap. The entire system operates at room temperature and the green fluorescence from erbium's characteristics is observed in our experiment. Using a bandpass filter from 2500 to 4500 nm to remove residual pump power, we measured the output optical spectra and average laser power by a Bristol 721 optical spectrum analyzer and an optical power meter (S425C-L, Thorlabs, Inc., Newton, NJ, USA), respectively. The radio-frequency spectra and waveforms of the gain-switched pulses were monitored by an electrical spectrum analyzer and an 1 GHz oscilloscope with an HgCdTe detector (Vigo PV1-4TE-6PIP).

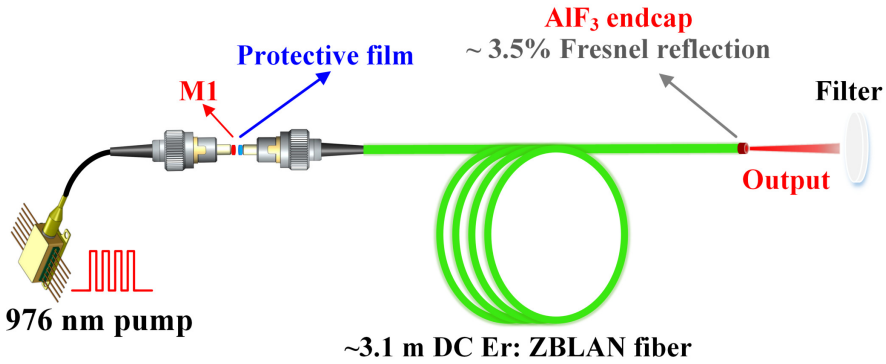

Figure 1. Experimental setup of all-fiber gain-switched Er^{3+}:ZBLAN laser at 2.8 μm.

The key techniques that determine the output performance of the laser are as follows. (1) The high-reflectivity FPM M1 with high damage threshold is favorable to high-power MIR laser operation, and the designed structure is shown in Figure 2a. Selecting Ta_2O_5 with high damage threshold (Ta_2O_5 > TiO_2) and SiO_2 to design and realize specific electric field manipulation of dielectric films is the key factor for accurate dichroic mirror and highly resistant M1. A 105/125 μm fiber with pigtail is firstly prepared to be a standard FC/PC fiber connector. After the end facet of the FC/PC fiber connector is finely polished by a commercial polishing machine, the M1 without any defect is uniformly deposited on it by ion beam-assisted deposition system. The reflectivity measured of M1 is as high as 98.4% at 2.8 μm, and the transmittance reaches 98.8% at 976 nm [see Figure 2b]. (2) The protective film of 600 nm thick Ta_2O_5 is directly coated on the well-cleaved input end facet of the DC Er^{3+}:ZBLAN fiber, mitigating the tip photodegradation caused by the strong absorption of water vapor at 3 μm laser; the microscopic image is shown in Figure 2c. The optical thickness of the single-layer Ta_2O_5 is calculated by the formula $ndcos\theta = 1/2(m\lambda)$ [m = 1, 2, 4, 6 · · ·], where n = 2.1 (the refractive index of Ta_2O_5), $\theta = 90°$ (the angle between laser transmission and the end facet: vertical transmission), m = 1, λ is the laser wavelength (~2800 nm), and therefore, the optical thickness d is about 666 nm. Considering a high transmittance at the pump wavelength, the optical thickness was further adjusted to ~600 nm, satisfying experimental requirements as much as possibles. As given in Figure 2d, the transmittance at 976 nm and 2.8 μm is as high as 95.6% and 93.5%, respectively. (3) Using a fusion splicer LFS4100 from Vytran, the perpendicularly cleaved 200/240 μm AlF_3-based endcap fusion-spliced to the output tip of Er^{3+}:ZBLAN fiber ensures better heat conduction (see Figure 2e), effectively reducing the power fluctuation from 0.61% to less than 0.5% at high power output. It is worth mentioning that AlF_3-based glass shows lower permeability to OH^- contamination and higher damage threshold than ZrF_4 fiber, so that can be effectively used as a fiber protective enclosure. The techniques above complement each other, laying the foundation for the 2.8 μm all-fiber high-power and high-energy gain-switched laser.

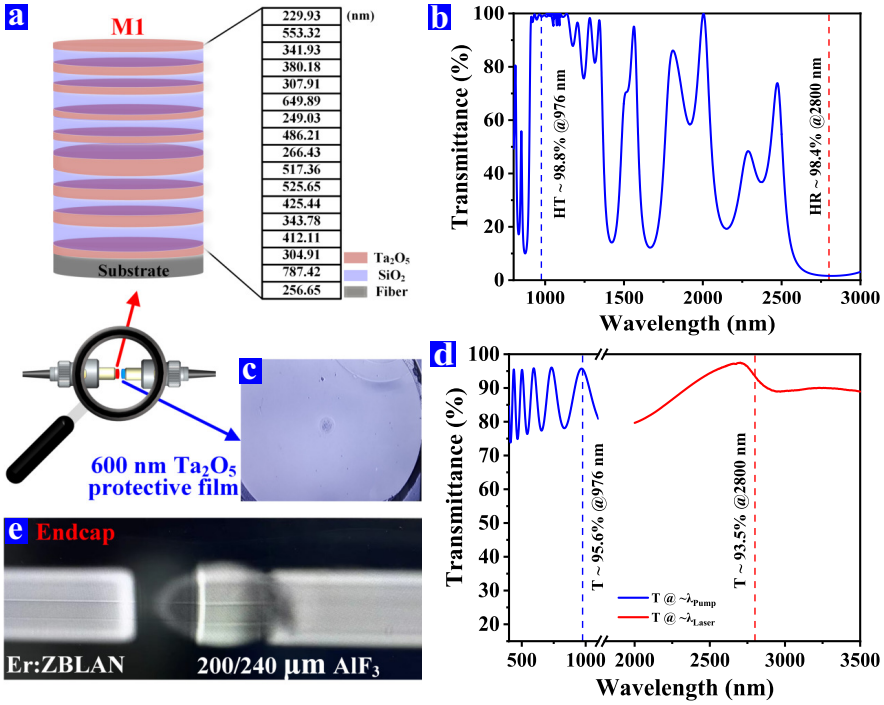

Figure 2. (**a**) The designed structure of the 105/125 μm FPM M1. (**b**) The transmission spectrum of the M1. (**c**) The microscope photograph and (**d**) the transmission spectrum of the protective film. (**e**) The AlF_3-based endcap fusion-spliced to Er^{3+}:ZBLAN fiber.

3. Results and Discussion

In experiment, we firstly studied the establishment of the 2.8 μm all-fiber gain-switched laser when the 976 nm pump average power increased. The pulse width of the 976 nm pump was set at 16 μs and the repetition rate was adjusted from 5 to 20 kHz. Once the average pump power reached a threshold, the laser pulsed signal was generated at the tail edge of the pump pulse (see the inset of Figure 3a). Figure 3a gives the typical pulsed laser spectra at the different pumping repetition rates, and the peak wavelengths located near 2.8 μm. At different pumping repetition rates, two kinds of single-pulse waveforms were detected in succession when the average pump power continuously increased, which could be called the "2−1" state and "1−1" state, respectively, as plotted in the inset of Figure 3b. The evolutions of the two operating states show their strong correlation with pump pulse energy, and Figure 3b shows the corresponding threshold pump energy, respectively. At a level of low pump energy, the energy for the population inversion of a single laser pulse required two pump pulses to provide. Thus, a single laser pulse occurred within twice the pump pulse period ("2−1" state). When the pump energy was increased to the threshold at which one laser pulse can be excited by one pump pulse, the laser pulse was generated almost simultaneously with the pump pulse ("1−1" state). The phenomenon was observed at the repetition rates of 5/10...18/20 kHz. It was observed that the threshold power energy required to establish the two operating states reduced with increasing pumping repetition rate, i.e., from about 27.4/36.8 μJ (5 kHz) to 11.2/18.5 μJ (20 kHz) of the "2−1"/"1−1" state, which can be interpreted as the fact that the shorter pumping cycle with increasing pumping repetition rate makes the populations remain easier in the upper laser level $^4I_{11/2}$ of Er^{3+}. Figure 3c indicates the output pulsed characteristics of "1−1" single-pulse output at different pump repetition rates and pump widths. As the pump repetition rate increased, it can be seen in the trend that the single-pulse energy decreased (red points), the single-pulse peak power also decreased (blue points), while the single-pulse width increased (black points). When the 976 nm pump was set at 16 μs/5 kHz, the 2.8-μm maximum single-pulse energy, peak power, and minimum pulse width obtained in our experiment were 4.8 μJ, 10.04 W, and 426 ns, respectively. It should be noted that although

the repetition rate of the pump in our experiment is adjustable between 20 Hz and 20 kHz, the threshold pump power was too high when the repetition frequency was <5 kHz, which was not conducive to the high-power output operation of the gain-switched fiber laser.

Nonetheless, further scalability of the single-pulse power and energy at 16 µs/5 kHz cannot be achieved simply by increasing pump power. When the pump power reached a larger value than 0.278 W, we observed that the output immediately switched to the pulse-burst operation, and it also should be considered as a chaotic oscillation state. Rather, the operating state of the pulse burst appeared; see the inset of Figure 3d. The quite chaotic temporal characteristics of the output are related to mode-hopping and mode competition [36]. When the pump power was increased slightly more than 0.278 W, the second and even the third pulses were generated because the pump energy became too large for the first pulse to fully extract the energy stored in the gain fiber, that is, in the pulse-burst state. As illustrated in Figure 3d, we give the output power/energy as a function of pump average power. In this case, the output power of the pulse burst increases linearly with the increased pump power. A maximum average pulse-burst power up to 0.410 W with a slope efficiency of 24.3% was obtained at the average pump power of 1.898 W, and the maximum energy of the pulse burst was 82 µJ.

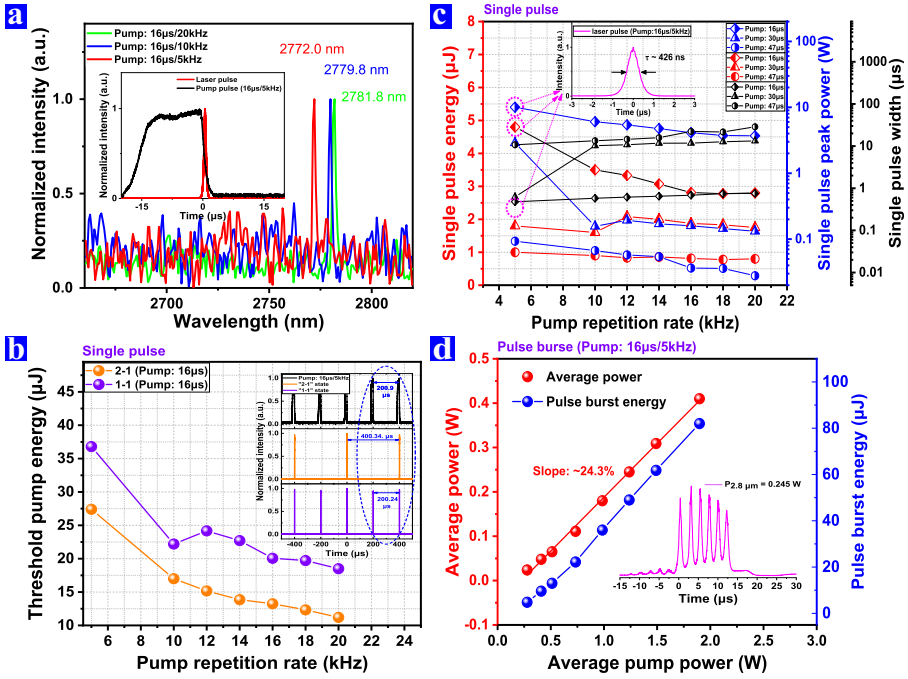

Figure 3. (**a**) Output spectra of the 2.8 µm all-fiber gain-switched Er^{3+}: ZBLAN laser (inset: single-pulse waveforms of laser and pump). (**b**) Threshold characteristic at different pumping repetition rates (pump setting: 16 µs). (**c**) The single-pulse characteristic at different pumping repetition rates and pulse widths (inset: the pulsed waveforms of pump and "2−1", "1−1" states). (**d**) The pulse-burst output power/energy as a function of average pump power (inset: the pulse-burst waveform at $P_{pulse\ burst}$ = 0.245 W (pump setting: 16 µs/5 kHz)).

In brief, when the pump power (energy) continuously increased, the two states of single-pulse and pulse-burst output can be attained for the all-fiber mid-infrared gain-switched laser. With the increase in pulsed pump power, which is essentially the increase in energy, we found that the gain-switched pulse sequence gradually changed from a single-pulse state to a pulse-burst state with multiple sub-pulses. This phenomenon is closely related to the pump energy delivered into the gain fiber. When the pump energy is at a relatively low level, there is only enough energy for the generation of a single-pulse output. While the pump pulse energy was higher than a certain value, the pulse-burst state occurred, which may be explained by the fact that after the emission of the first gain-switched pulse,

the residual pump energy stored in the gain fiber could drive the upper-level population back above the pulse threshold again, and then the excited population becomes too large to be depleted by the first gain-switched pulse, thus causing gain-switched pulses to break into double pulses. As the pump pulse energy further increased, the energy stored in the second pulse increased gradually, until a third sub-pulse was generated to share the energy stored by the second pulse and so forth; then, the pulse burst (multi-pulses) is output.

Figure 4 gives the temporal characteristics of two states "2−1" and "1−1" mentioned in Figure 3 at different pumping repetition rates. According the Figure 4a, the time intervals of the "2−1" states decreased from 400.40 µs to 100.11 µs, corresponding to the pumping repetition rate from 5 kHz to 20 kHz with slightly fluctuating amplitudes, and the time intervals were always twice as much as that of the pump pulse at different pumping repetition rates. It can be inferred that at a low power (energy) level, the energy of one pump pulse cannot excite a population inversion for a laser pulse, so a single pulse of a laser cannot be generated in one pump period. A single pulse can be generated until the second pump pulse is delivered into the gain fiber to provide enough energy for population inversion. At this time, the single pulse was excited by two pump pulses, i.e., "2−1" state. As shown in Figure 4b, the time intervals of "1−1" single-pulse state were monitored from 200.16 µs to 50.05 µs with the increasing 5–20 kHz, and they were basically the same as the time intervals of pump pulse, that is, every pump pulse produced one gain-switched single pulse. It can be interpreted that compared to the "2−1" state, the higher threshold pump energy required by the "1−1" state is sufficient to support a population inversion within a pulse period of pump.

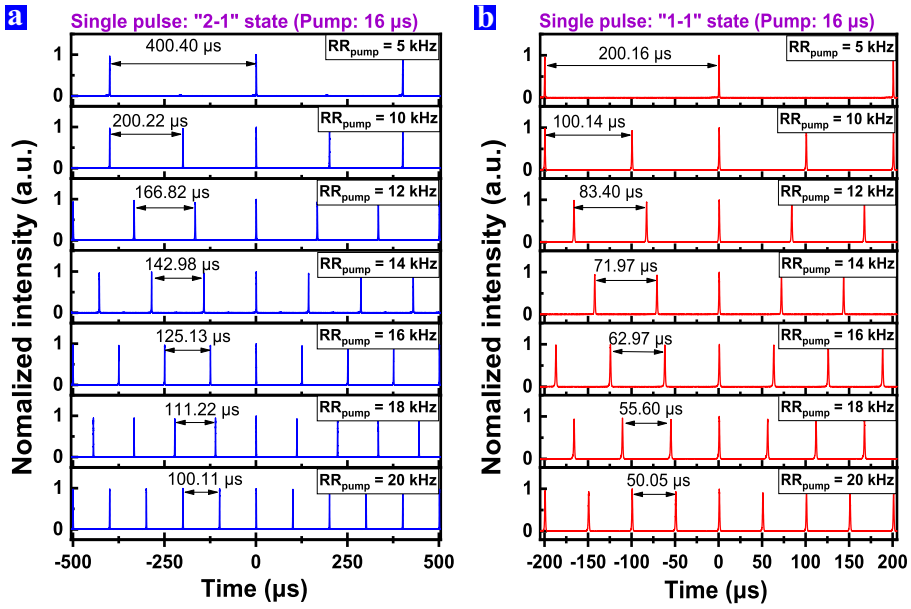

Figure 4. Temporal characteristics of single pulse at different pump repetition rates (pump setting: 16 µs). (**a**) The "2−1" state and (**b**) "1−1" state .

The output characteristics of pulse burst with increasing output power (pump setting: 16 µs/5 kHz) are shown in Figure 5. When the laser output >0.024 W, the MIR all-fiber gain-switched laser operated at pulse-burst regime. As the average power of pulse burst increased from 0.047 W to 0.410 W, the number of sub-pulses increased from 2 to 8; see Figure 5a. The output spectra given in Figure 5b reveal the drift of the central wavelength range toward a longer wavelength (from 2762.0 nm to 2793.1 nm) in a wide wavelength range; it was attributed to reabsorption of laser emission at shorter wavelengths.

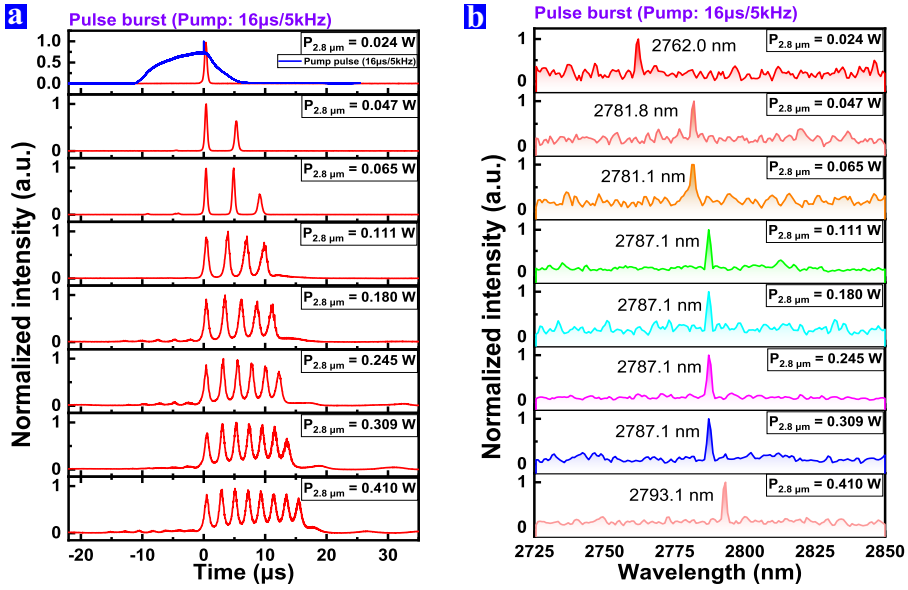

Figure 5. Output characteristics of pulse burst with increasing output power (pump setting: 16 μs/5 kHz). (**a**) Temporal characteristic and (**b**) output spectra.

The output power stability of the laser system at the pump setting of 16 μs/5 kHz was assessed over 30 min continuously, as shown in Figure 6a. When the laser operated in pulse-burst state and the average output power was ~0.410 W, the laser showed a fluctuation from 0.41 to 0.43 W, with a power fluctuation of 1.01%. At the average power of 0.410 W, the RF spectrum was tested, as shown in Figure 6b, and the RF signal-to-noise ratio (SNR) was over 25.1 dB at the fundamental frequency of the laser pulse located at 5 kHz.

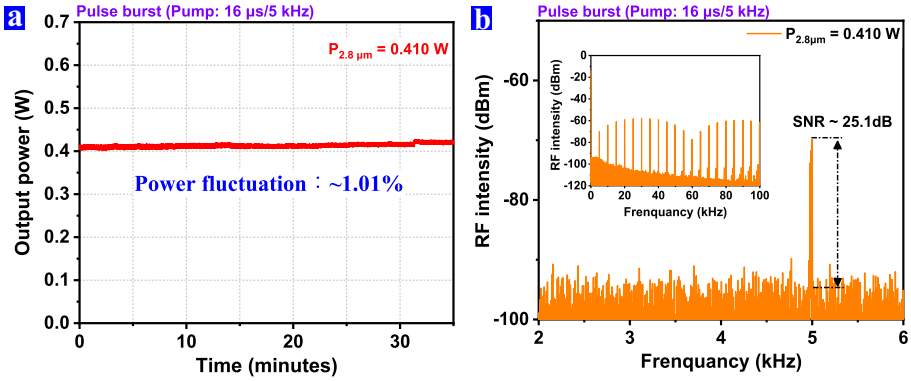

Figure 6. (**a**) The average power stability and (**b**) the RF spectrum at 0.410 W of 2.8 μm all-fiber Er^{3+}:ZBLAN gain-switched laser (pump setting: 16 μs/5 kHz).

Due to the fact that the highest average pump power that could be provided by the pump setting was 20 kHz/47 μs, we adjusted the pump at 20 kHz/47 μs to enlarge the laser pulse-burst power/energy. The corresponding output performance is plotted in Figure 7. The threshold pump power of pulse burst is about 0.457 W, and the average power and energy of the pulse burst increase linearly with the average pump power. A maximum average pulse-burst power of 5.291 W was obtained at the average pump power of 21.2 W; the slope efficiency is determined to be about 25.2%, and the highest energy of the pulse burst is 264.55 μJ. Using the image display function of the power meter (Thorlabs), we also monitored the stability of the laser system over 30 min when the pulse-burst output power was ~4.23 W. The average power fluctuation was less than 0.49%, there was no downward trend in power, and the end facets of the fluoride fiber were intact, indicating the good stability of our gain-switched laser system.

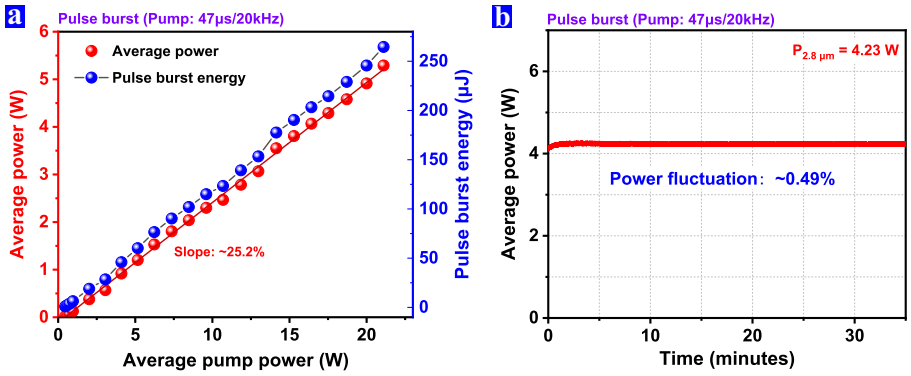

Figure 7. (**a**) The 2.8 μm power/energy and (**b**) average power stability of the pulse-burst output (pump setting: 47 μs/20 kHz).

The pulse-burst characteristics (pump setting: 47 μs/20 kHz) were investigated by monitoring the pulsed trains, laser spectra, and broadband RF output spectra; the results are depicted in Figure 8. According to Figure 8a, if the average pump power is less than 0.457 W (the average laser power < 0.02 W), the stable single- pulse operation can be maintained. As the average pump power further increased, a second and even more sub-pulses occurred, namely pulse bursts. The corresponding spectra are shown in Figure 8b, with the laser power (pump power) increased from 0.020 W (0.457 W) to 5.291 W (21.2 W), and the laser central wavelength red-shifted from 2780.4 nm to 2799.2 nm due to the reabsorption effect. As shown in Figure 8c, the modulations of RF spectra intensity in multi-pulse states were distinctly different from the single-pulse state, which agreed with the Fourier transform of multiple sub-pulses, and the RF SNR was approximately 25 dB at the fundamental frequency of 20 kHz.

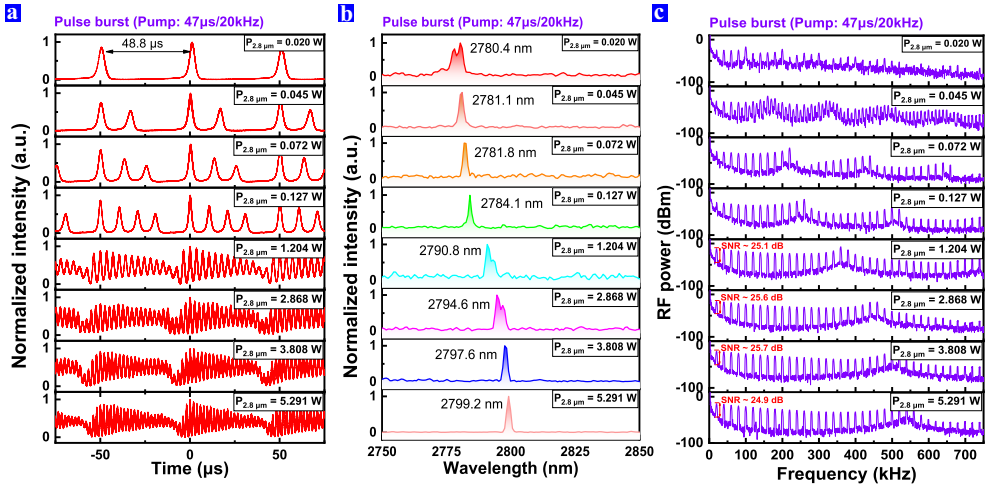

Figure 8. Output pulse-burst characteristics under pump setting of 47 μs/20 kHz. (**a**) The evolution of gain-switched pulse-burst waveforms. (**b**) Typical output optical spectra. (**c**) Broadband RF output spectra.

4. Conclusions

In summary, utilizing the home-made dielectric fiber pigtail mirror and fiber-tip protection (e.g., protective film and AlF_3-based endcap), we demonstrated a 2.8 μm all-fiber high-power and high-energy gain-switched Er^{3+}:ZBLAN laser operating in two different states of single pulse and pulse burst. The evolutions of the two states, influenced by pulse width, pumping repetition rate, and pump power, were investigated in detail. The shortest single pulse of 426 ns with maximum single-pulse energy of 4.8 μJ was attained at pump setting of 16 μs/5 kHz. When the 976 nm pump is set at 16 μs/5 kHz and

47 μs/20 kHz, respectively, a 2.8 μm maximum power (energy) of 0.410 W (82 μJ) and 5.291 W (264.55 μJ) from pulse-burst output can be obtained. Technically, the output energy of single pulse could be scaled up by reducing the pump duty cycle, and the higher output power and energy of pulse burst could be obtained by using a longer gain fiber. Compared with the fusion-splicing technology with fluoride FBG, this work may provide an alternative solution for realizing easily available and low-cost MIR all-fiber gain-switched laser with high power and high energy.

Author Contributions: Conceptualization, T.C. and Z.L.; methodology, T.C. and W.Z.; investigation, J.S. and L.H.; data curation, T.C. and L.H.; formal analysis, T.C.; writing—original draft preparation, T.C.; writing—review and editing Z.L and T.C.; supervision, Z.L. and J.L. resources, Z.L. and Y.D. and Y.B.; project administration, Y.B., Z.L. and J.L. All authors have read and agreed to the published version of the manuscript.

Funding: This research was funded by National Natural Science Foundation of China (grant number 62375231) and Natural Science Foundation of Fujian Province under Grant 2022J02007.

Institutional Review Board Statement: Not applicable.

Informed Consent Statement: Not applicable.

Data Availability Statement: The data provided in this study are available upon request from the corresponding author.

Conflicts of Interest: The authors declare no conflicts of interest.

Abbreviations

The following abbreviations are used in this manuscript:

MIR	mid-infrared
AR	anti-reflection
FPM	fiber pigtail mirror
LD	laser diode
DC	double cladding
SNR	signal-to-noise ratio

Appendix A

Table A1. The reports on gain-switched fiber lasers in the 3–3.5 μm spectral region.

Year	Institution	Wavelength	Gain Fiber	Structure	Power/Energy	Efficiency
2001 [22]	UoM	2.7 μm	Er^{3+}:ZBLAN	Free space	1.9 mJ	13.5%
2011 [23]	Uni. of Ljubljana	2.8 μm	Er^{3+}:ZBLAN	Free space	2 W	34%
2017 [25]	UESTC	2.699–2.869 μm	Er^{3+}:ZBLAN	Free space	473.3 mW	-
2018 [24]	Université Laval	2.826 μm	Er^{3+}:ZBLAN	**All fiber**	**11.20 W /80 μJ**	28%
2018 [26]	Université Laval	3.55 μm	Er^{3+}:ZBLAN	Free space	180 μJ	4.7%
2018 [27]	UESTC	3.46 μm	Er^{3+}:ZBLAN	Free space	1.04 W/10.4 μJ	24.6%
2018 [28]	Macquarie Uni.	2.8–3.4 μm	Dy^{3+}:ZBLAN	Free space	170 mW	21%
2018 [31]	UESTC	2.895–3.0 μm	Ho^{3+}:ZBLAN	Free space	389.3 mW/4.87 μJ	10.8%
2019 [29]	UESTC	2.8–3.1 μm	Dy^{3+}:ZBLAN	Free space	218.6 mW/2.73 μJ	9.4%
2020 [30]	Université Laval	3.24 μm	Dy^{3+}:ZBLAN	Free space	1.43 W/19.2 μJ	22%
2020 [32]	Xiamen uni.	2.92 μm	Ho^{3+}:ZBLAN	**All fiber**	54.2 mW	10.12%

References

1. Yumoto, M.; Saito, N.; Lin, T.; Kawamura, R.; Aoki, A.; Izumi, Y.; Wada, S. High-energy, nanosecond pulsed Cr: CdSe laser with a 2.25–3.08 μm tuning range for laser biomaterial processing. *Biomed. Opt. Express* **2018**, *9*, 5645–5653. [CrossRef] [PubMed]
2. Garcia-Lechuga, M.; Casquero, N.; Wang, A.; Grojo, D.; Siegel, J. Deep silicon smorphization induced by femtosecond laser pulses up to the mid-infrared. *Adv. Opt. Mater.* **2021**, *9*, 2100400. [CrossRef]
3. Kerse, C.; Kalaycıoğlu, H.; Elahi, P.; Çetin, B.; Kesim, D.K.; Akçaalan, Ö.; Yavaş, S.; Aşık, M.D.; Öktem, B.; Heinar, T.; et al. Ablation-cooled material removal with ultrafast bursts of pulses. *Nature* **2016**, *537*, 84–88. [CrossRef] [PubMed]
4. Caballero-Lucas, F.; Obata, K.; Sugioka, K. Enhanced ablation efficiency for silicon by femtosecond laser microprocessing with GHz bursts in MHz bursts (BiBurst). *Int. J. Extrem. Manuf.* **2022**, *4*, 015103. [CrossRef]

5. Lambert-Girard, S.; Allard, M.; Piché, M.; Babin, F. Differential optical absorption spectroscopy lidar for mid-infrared gaseous measurements. *Appl. Opt.* **2015**, *54*, 1647–1656. [CrossRef]
6. Refaat, T.F.; Singh, U.N.; Petros, M.; Remus, R.; Yu, J. Self-calibration and laser energy monitor validations for a double-pulsed 2-μm CO_2 integrated path differential absorption lidar application. *Appl. Opt.* **2015**, *54*, 7240–7251. [CrossRef] [PubMed]
7. Li, X.; Luo, P. Boosting ranging performance of LiDAR using multi-pulse coherent average. *IEEE Sens. J.* **2019**, *15*, 6270–6278. [CrossRef]
8. Holcomb, J.D. Versatility of erbium YAG laser: From fractional skin rejuvenation to full-field skin resurfacing. *Facial Plast. Surg. Clin.* **2011**, *19*, 261–273. [CrossRef] [PubMed]
9. Stübinger, S. Advances in bone surgery: The Er: YAG laser in oral surgery and implant dentistry. *Clin. Cosmet. Inv. Dent.* **2010**, *2*, 47–62. [CrossRef]
10. Pratisto, H.; Frenz, M.; Ith, M.; Altermatt, H.J.; Jansen, E.D.; Weber, H.P. Combination of fiber-guided pulsed erbium and holmium laser radiation for tissue ablation under water. *Appl. Opt.* **1996**, *35*, 3328–3337. [CrossRef]
11. Bekman, H.T.;Van Den Heuvel, J.C.; Van Putten, F.J.M.; Schleijpen, R. Development of a mid-infrared laser for study of infrared countermeasures techniques. In Proceedings of the European Symposium on Optics and Photonics for Defence and Security, London, UK, 29 December 2004; Technologies for Optical Countermeasures; pp. 27–38.
12. Wang, X.; Hu, Q.; Wang, Y. Study of mid-infrared laser jamming effect on reticle-based seekers. In Proceedings of the Seventeenth National Conference on Laser Technology and Optoelectronics, Shanghai, China, 23–26 August 2022; pp. 380–383.
13. Coleman, D.J.; King, T.A.; Ko, D.-K.; Lee, J. Q-switched operation of a 2.7 μm cladding-pumped Er^{3+}/Pr^{3+} codoped ZBLAN fibre laser. *Opt. Commun.* **2004**, *236*, 379–385. [CrossRef]
14. Hu, T.; Hudson, D.D.; Jackson, S.D. Actively Q-switched 2.9 μm $Ho^{3+}Pr^{3+}$-doped fluoride fiber laser. *Opt. Lett.* **2012**, *37*, 2145–2147. [CrossRef] [PubMed]
15. Tokita, S.; Murakami, M.; Shimizu, S.; Hashida, M.; Sakabe, S. 12 W Q-switched Er: ZBLAN fiber laser at 2.8 μm. *Opt. Lett.* **2011**, *36*, 2812–2814. [CrossRef] [PubMed]
16. Li, J.; Hu, T.; Jackson, S.D. Dual wavelength Q-switched cascade laser. *Opt. Lett.* **2012**, *37*, 2208–2210. [CrossRef] [PubMed]
17. Woodward, R.I.; Majewski, M.R.; Macadam, N.; Hu, G.; Albrow-Owen, T.; Hasan, T. and Jackson, Stuart D. Q-switched Dy:ZBLAN fiber lasers beyond 3 μm comparison of pulse generation using acousto-optic modulation and inkjet-printed black phosphorus. *Opt. Express* **2019**, *27*, 15032–15045. [CrossRef] [PubMed]
18. Lü, Y.; Wei, C.; Zhang, H.; Kang, Z.; Qin, G.; Liu, Y. Wideband tunable passively Q-switched fiber laser at 2.8 μm using a broadband carbon nanotube saturable absorber. *Photonics Res.* **2019**, *7*, 14–18. [CrossRef]
19. Qin, Z.; Xie, G.; Zhang, H.; Zhao, C.; Yuan, P.; Wen, S.; Qian, L. Black phosphorus as saturable absorber for the Q-switched Er: ZBLAN fiber laser at 2.8 μm. *Opt. Express* **2015**, *23*, 24713–24718. [CrossRef] [PubMed]
20. Kang, Z.; Liu, M.; Li, Z.; Li, S.; Jia, Z.; Liu, C.; Qin, W.; Qin, G. Passively Q-switched erbium doped fiber laser using a gold nanostars based saturable absorber. *Photonics Res.* **2018**, *6*, 549–553. [CrossRef]
21. Wei, C.; Zhu, X.; Norwood, R.A.; Peyghambarian, N. Passively Q-switched 2.8-μm nanosecond fiber laser. *IEEE Photonics Technol. Lett.* **2012**, *24*, 1741–1744. [CrossRef]
22. Dickinson, B.C.; Golding, P.S.; Pollnau, M.; King, T.A.; Jackson, S.D. Investigation of a 791-nm pulsed-pumped 2.7-μm Er-doped ZBLAN fibre laser. *Opt. Commun.* **2001**, *191*, 315–321. [CrossRef]
23. Gorjan, M.; Marinček, M.; Čopič, M. High-power pulsed diode-pumped Er: ZBLAN fiber laser. *Opt. Lett.* **2011**, *36*, 1923–1925. [CrossRef] [PubMed]
24. Paradis, P.; Fortin, V.; Aydin, Y.O.; Vallée, R.; Bernier, M. High-power pulsed diode-pumped Er: ZBLAN fiber laser. *Opt. Lett.* **2018**, *43*, 3196–3199. [CrossRef] [PubMed]
25. Wei, C.; Luo, H.; Shi, H.; Lyu, Y.; Zhang, H.; Liu, Y. Widely wavelength tunable gain-switched Er^{3+}-doped ZBLAN fiber laser around 2.8 μm. *Opt. Express* **2017**, *25*, 8816–8827. [CrossRef] [PubMed]
26. Jobin, F.; Fortin, V.; Maes, F.; Bernier, M.; Vallée, R. Gain-switched fiber laser at 3.55 μm. *Opt. Lett.* **2018**, *43*, 1770–1773. [CrossRef]
27. Luo, H.; Yang, J.; Liu, F.; Hu, Z.; Xu, Y.; Yan, F.; Peng, H.; Ouellette, F.; Li, J.; Liu, Y. Watt-level gain-switched fiber laser at 3.46 μm. *Opt. Express* **2018**, *27*, 1367–1375. [CrossRef] [PubMed]
28. Majewski, M.R.; Woodward, R.I.; Jackson, S.D. Dysprosium-doped ZBLAN fiber laser tunable from 2.8 μm to 3.4 μm, pumped at 1.7 μm. *Opt. Lett.* **2018**, *43*, 971–974. [CrossRef]
29. Luo, H.; Xu, Y.; Li, J.; Liu, Y. Gain-switched dysprosium fiber laser tunable from 2.8 to 3.1 μm. *Opt. Express* **2019**, *27*, 27151–27158. [CrossRef] [PubMed]
30. Jobin, F.; Paradis, P.; Fortin, V.; Magnan-Saucier, S.; Bernier, M.; Vallée, R. 1.4 W in-band pumped Dy^{3+}-doped gain-switched fiber laser at 3.24 μm. *Opt. Lett.* **2020**, *45*, 5028–5031. [CrossRef]
31. Luo, H.; Li, J.; Hai, Y.; Lai, X.; Liu, Y. State-switchable and wavelength-tunable gain-switched mid-infrared fiber laser in the wavelength region around 2.94 μm. *Opt. Express* **2018**, *26*, 63–79. [CrossRef]
32. Zhang, X.; Li, W.; Li, J.; Xu, H.; Cai, Z.; Luo, Z. Mid-infrared all-fiber gain-switched pulsed laser at 3 μm. *Opto-Electron. Adv.* **2020**, *3*, 190032. [CrossRef]
33. Caron, N.; Bernier, M.; Faucher, D.; Vallée, R. Understanding the fiber tip thermal runaway present in 3 μm fluoride glass fiber lasers. *Opt. Express* **2012**, *20*, 22188–22194. [CrossRef]

34. Pushkin, A.V.; Migal, E.A.; Uehara, H.; Goya, K.; Tokita, S.; Frolov, M.P.; Korostelin, Y.V.; Kozlovsky, V.I.; Skasyrsky, Y.K.; Potemkin, F.V. Compact, highly efficient, 2.1-W continuous-wave mid-infrared Fe: ZnSe coherent source, pumped by an Er: ZBLAN fiber laser. *Opt. Lett.* **2012**, *43*, 5941–5944. [CrossRef] [PubMed]
35. Rayner, A.; Hirsch, M.; Heckenberg, N.R.; Rubinsztein-Dunlop, H. Distributed laser refrigeration. *Appl. Opt.* **2001**, *40*, 5423–5429. [CrossRef] [PubMed]
36. Le Flohic, M.; Franchois, P.-L.; Allain, J.-Y.; Sanchez, F.; Stephan, G.M. Dynamics of the transient buildup of emission in Nd^{3+}-doped fiber lasers. *IEEE J. Quantum Electron.* **1991**, *27*, 1910–1921. [CrossRef]